

C-arm flat detector computed tomography parenchymal blood volume imaging: the nature of parenchymal blood volume parameter and the feasibility of parenchymal blood volume imaging in aneurysmal subarachnoid haemorrhage patients

Mudassar Kamran¹ · James V. Byrne¹

Received: 13 February 2015 / Accepted: 19 May 2015 / Published online: 29 May 2015
© Springer-Verlag Berlin Heidelberg 2015

Abstract

Introduction C-arm flat detector computed tomography (FDCT) parenchymal blood volume (PBV) measurements allow assessment of cerebral haemodynamics in the neurointerventional suite. This paper explores the feasibility of C-arm computed tomography (CT) PBV imaging and the relationship between the C-arm CT PBV and the MR-PWI-derived cerebral blood volume (CBV) and cerebral blood flow (CBF) parameters in aneurysmal subarachnoid haemorrhage (SAH) patients developing delayed cerebral ischemia (DCI). **Methods** Twenty-six patients with DCI following aneurysmal SAH underwent a research C-arm CT PBV scan using a bi-plane angiography system and contemporaneous MR-PWI scan as part of a prospective study. Quantitative whole-brain atlas-based volume-of-interest analysis in conjunction with Pearson correlation and Bland-Altman tests was performed to explore the agreement between C-arm CT PBV and MR-derived CBV and CBF measurements.

Results All patients received medical management, while eight patients (31 %) underwent selective intra-arterial chemical angioplasty. Colour-coded C-arm CT PBV maps were 91 % sensitive and 100 % specific in detecting the perfusion abnormalities. C-arm CT rPBV demonstrated good agreement and strong correlation with both MR-rCBV and MR-rCBF measurements; the agreement and correlation were stronger for MR-rCBF relative to MR-rCBV and improved for C-arm

CT PBV versus the geometric mean of MR-rCBV and MR-rCBF. Analysis of weighted means showed that the C-arm CT PBV has a preferential blood flow weighting (≈ 60 % blood flow and ≈ 40 % blood volume weighting).

Conclusions C-arm CT PBV imaging is feasible in DCI following aneurysmal SAH. PBV is a composite perfusion parameter incorporating both blood flow and blood volume weightings. That PBV has preferential (≈ 60 %) blood flow weighting is an important finding, which is of clinical significance when interpreting the C-arm CT PBV maps, particularly in the setting of acute brain ischemia.

Keywords Parenchymal blood volume · C-arm flat detector computed tomography · Subarachnoid haemorrhage · Cerebral blood flow · MR perfusion-weighted imaging

Introduction

Recent developments in flat detector equipped angiographic systems have made it possible to study cerebral haemodynamics in the neurointerventional suite [1]. C-arm rotational image datasets acquired with and without intravenous contrast administration are analysed using the principles of image subtraction and indicator dilution theory to generate quantitative voxel-wise maps of a parameter called parenchymal blood volume (PBV) [1]. Initial studies have compared the C-arm flat detector computed tomography (C-arm FDCT or C-arm CT) PBV with only the CTP-derived cerebral blood volume (CBV) measurements [2–5]. The C-arm CT PBV calculations are performed in a manner similar to that proposed for multi-detector CTA by Hamburg et al. [6]. For multi-detector CT, the CTA source images (CTA-SI) can be used

✉ Mudassar Kamran
m.kamran@oxon.org

¹ Nuffield Department of Surgical Sciences, University of Oxford, Room 6607, Level 6, John Radcliffe Hospital, Headington, Oxford OX3 9DU, UK

alone or be post-processed to generate colour-coded PBV maps [7–9]. Sharma et al. showed that despite theoretical models suggesting these images (CTA-SI or colour-coded CT PBV maps) to be predominately blood volume weighted, technique-related factors impart a preferential blood flow weighting to them [10]. However, whether the C-arm CT-derived PBV images are preferentially blood flow or blood volume weighted has not been studied.

Availability of C-arm CT PBV technique in the neurointerventional suite is of particular interest in patients with aneurysmal subarachnoid haemorrhage (SAH). Cerebral perfusion abnormalities have been shown to serve as an early diagnostic marker for delayed cerebral ischemia (DCI), the leading cause of morbidity and mortality in patients surviving the initial ictus of SAH [11–14]. For these patients, availability of C-arm CT PBV maps in the interventional suite could potentially be useful as a baseline assessment and in allowing early identification of cerebral perfusion abnormalities in the interventional suite, which if present could assist in planning an intervention without the need for patient transfer between the diagnostic and interventional suites.

This paper aimed to (1) investigate the relationship between C-arm CT PBV and the MR-PWI-derived CBV and cerebral blood flow (CBF) parameters and (2) explore the feasibility of C-arm CT PBV protocol scanning in patients with aneurysmal SAH who developed delayed clinical deterioration.

Materials and methods

With local research ethics committee approval, a series of patients ($n=26$) with aneurysmal SAH meeting the inclusion and exclusion criteria were enrolled in this prospective study.

Inclusion criteria were patients aged over 18 years with documented aneurysmal SAH who subsequently developed symptoms and signs suggesting DCI and requiring confirmatory imaging—a situation necessitating admission and management in neuro-intensive care unit (neuro-ICU). At our institution, SAH is diagnosed using non-contrast CT (NCCT) head or with cerebrospinal fluid (CSF) sampling by lumbar puncture when initial NCCT head is negative but clinical suspicion of SAH remains high, and is graded as described by Fisher et al. [15]. The diagnosis of DCI was based on clinical assessment by the multidisciplinary neuro-ICU team and was defined as clinical deterioration (focal neurological deficits or reduced level of consciousness) lasting 2 h or longer with no evidence of rebleed or hydrocephalus on NCCT head and no other medical causes such as infections or metabolic disturbances to explain the neurological deterioration.

Exclusion criteria were a history of allergy to iodinated contrast medium, renal impairment, pregnancy or contraindications to magnetic resonance (MR) examination. All recruited patients had undergone aneurysm repair by endovascular coil embolization. Written informed consents were obtained from patients or, if they were unable to complete the consent process, from a family member or a designated surrogate as defined by the research ethics committee approval for the study. Clinical records for all patients were collected and reviewed. The patients underwent a clinically indicated MRI examination using a protocol that included perfusion-weighted sequences concurrent with the research C-arm CT scan using PBV protocol. The imaging protocols and post-processing steps for the two imaging studies are described in the following sections. Additional subsequent imaging was performed as clinically indicated. Clinical and imaging data with patient-identifying information was anonymized and coded. Anonymised data was stored in a research database while the identifying variables were stored in a separate identification database; the two databases were linked through codes, which were accessible to the members of Oxford Neurovascular and Neuroradiology Research Unit (ONNRU) involved in this particular study, in accordance with the research ethics committee guidelines.

C-arm flat detector computed tomography imaging

C-arm FDCT scans were performed on a flat detector equipped biplane angiography system (Axiom Artis dBA; Siemens Healthcare, Germany) in the neurointerventional suite of Department of Neuroradiology, West Wing, John Radcliffe Hospital, Oxford, UK. The imaging protocol included two rotational acquisitions: the mask and the contrast-enhanced (or fill) runs. Projection data for each run was acquired using the following parameters: 419 projection images, 0.5° frame angle, 210° angular scan range, 8 s acquisition time and 0.36 μ Gy radiation dose per frame. The contrast-enhanced dataset was acquired following manually triggered intravenous injection of radiographic contrast material Niopam 370 (Bracco spa, Milan, Italy) using a power injector (Medrad, Inc., Philadelphia). The injection parameters were contrast concentration, 370 mg iodine/ml; volume, 80 ml; injection rate, 4 ml/s administered through the antecubital vein; injection pressure, 300 lb per square inch (psi) and injection duration, 20 s. Passage of contrast material through the cerebral vasculature was monitored on two-dimensional (2D) fluoroscopic images (2 frames/s) and the contrast-enhanced run was triggered when maximal opacification of the superior sagittal sinus was observed as described by Struffert et al. [5].

Post-processing of the data to generate colour-coded PBV maps was performed on a dedicated research workstation (Leonardo, Siemens AG, Healthcare) using a prototype software. Briefly, the steps involved in estimation of quantitative PBV measurements were (1) co-registration of the two volumes, the mask and the contrast-enhanced; (2) subtraction of the mask volume from the contrast-enhanced volume; (3) normalization of the subtracted data with an input function automatically estimated from the histogram analysis of vascular tree and (4) colour coding with a standard colour look-up table to generate the PBV colour-coded maps for visualization and interpretation [1]. The final PBV values were expressed in units of millilitres per 1000 ml of cerebral tissue. PBV values for the volume-of-interest (VOI) analysis were converted to more commonly used units of millilitres per 100 g using a simple conversion factor that takes into account the cerebral tissue density (1.05 g/ml). For visualization of the vessels, the contrast-enhanced dataset was reconstructed separately on a commercially available dedicated workstation (Leonardo, Siemens AG, Healthcare). Volumetric rendering technique (VRT) and maximum intensity projection (MIP) reconstructions were used to evaluate the cerebral vasculature. CT-like soft tissue reconstructions were obtained in all cases.

Magnetic resonance imaging

A standard MR scan protocol comprising axial and sagittal T1-weighted, axial T2-weighted, diffusion-weighted, perfusion-weighted and time-of-flight (TOF) angiography sequences was performed on Philips Achieva 1.5-T MRI unit. The sequence details and the parameters used for each sequence are discussed below.

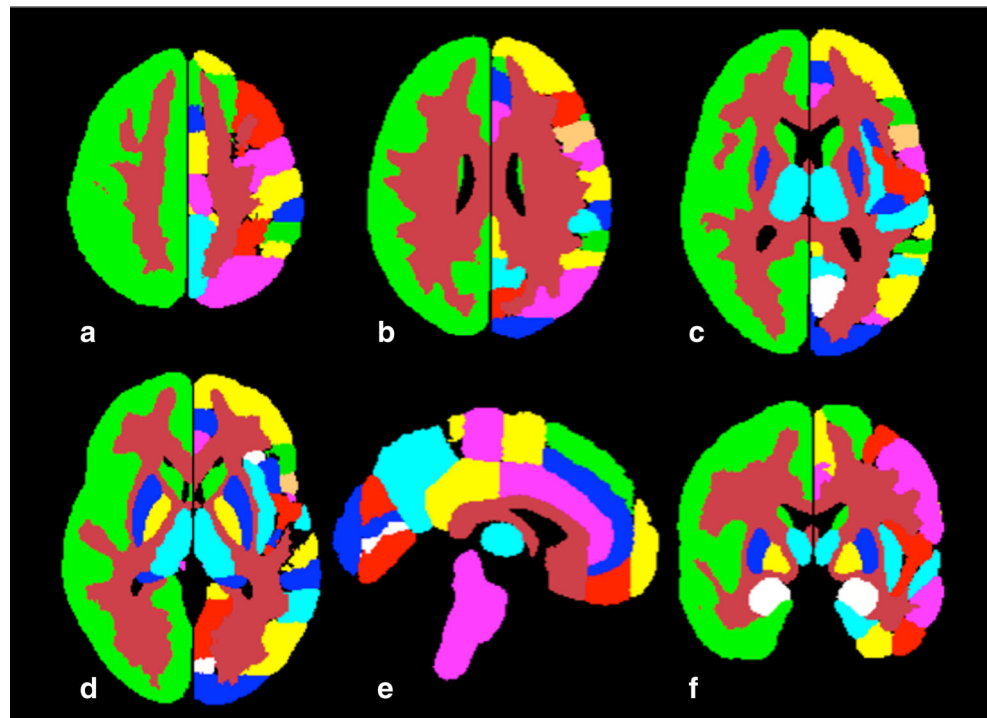
1. *Sagittal T1-weighted*: Repetition time (TR) 700 ms, time-to-echo (TE) 16 ms, field-of-view (FOV) 149×252 mm, reconstruction matrix 480×480, slices 25, slice thickness 5 mm, voxel size 0.53×0.53×5 mm and sequence duration 2 min 32 s.
2. *Axial T1-weighted post-Gadolinium*: TR 704 ms, TE 16 ms, FOV 176×250, reconstruction matrix 512×512, slices 25, slice thickness 5 mm, voxel size 0.49×0.49×5 mm and sequence duration 2 min 22.2 s.
3. *Axial T2-weighted*: TR 5061 ms, TE 100ms, FOV 174×250 mm, reconstruction matrix 512×512, slices 25, slice thickness 5 mm, voxel size 0.65×0.65×5 mm and sequence duration 2 min 36 s.
4. *Diffusion-weighted*: TR 2897 ms, TE 73 ms, FOV 174×249 mm, reconstruction matrix 144×144, slices 25, slice thickness 5 mm, voxel size 1.74×1.73×5 mm, *b* values 0 and 1000, EPI factor 51 and sequence duration 34 s.
5. *TOF angiography*: TR 26 ms, TE 6.9 ms, FOV 200×200 mm, reconstruction matrix 512×512, slices 140, slice thickness 0.5 mm, voxel size 0.39×0.39×0.5 mm and sequence duration 6 min 14.4 s.
6. *Perfusion-weighted*: Perfusion data was acquired using the dynamic susceptibility contrast (DSC) technique with the following parameters: T2*-weighted gradient-echo echoplanar sequence, TR 2000 ms, TE 44 ms, FOV 248×248 mm, reconstruction matrix 256×256, voxel size 0.98×0.98×4 mm, SENSE factor 2.1, bandwidth 806 Hz/pixel and sequence duration 1 min 46 s. Paramagnetic contrast material was administered intravenously with an MR-compatible power injector (Medrad, Inc.) at 5 ml/s followed by 10 ml saline flush. Fifteen slices covering the whole brain were acquired at 50 time points following the injection of 0.2 mmol/kg of Gadopentate (Prohance, Bracco Diagnostics, Inc., Italy).

Post-processing of the perfusion data was performed using a commercially available software (nordicICE perfusion package, NordicNeuroLab, Bergen, Norway), both CE marked and FDA approved. After motion correction of the raw data, perfusion maps were created using the standard singular value deconvolution (SVD) technique. Arterial input function (AIF) to deconvolve the dynamic tissue response curve was automatically determined and SVD regularization was achieved with the truncated SVD approach (cut-off fraction 0.20) and iterative thresholding (target oscillation index 0.10). Semi-quantitative, leakage-corrected output perfusion maps for clinical interpretation included cerebral blood flow (CBF), cerebral blood volume (CBV), mean transit time (MTT) and time to peak (TTP).

Further post-processing and quantitative VOI analysis

Quantitative/semi-quantitative parametric perfusion maps for the two techniques were further post-processed using the FMRIB software library (FSL) tools [16]. Brain extraction tool (BET) was used to delete the non-brain tissues from the images of interest [17]. Linear registration of the C-arm PBV maps and the MR perfusion parametric maps (CBF, CBV and MTT) for each patient was performed to the T1-weighted average structural template brain volume in the MNI152 space with FMRIB linear image registration tool (FLIRT) [18]. Binarized predefined cortical and subcortical volumes of interest (VOIs), as defined in the Harvard-Oxford structural brain atlas, were applied to the co-registered parametric maps. The 56 VOIs used for each hemisphere are depicted in Fig. 1. Mean, median and standard deviation values of each parameter were extracted for all VOIs encompassing both hemispheres. Given the semi-quantitative nature of MR-PWI measurements, we decided to use the interhemispheric ratios of all parameters for comparison. The interhemispheric ratios for MR-CBF, MR-CBV and C-arm CT PBV were calculated (e.g. right PBV/left PBV=relative PBV or rPBV) using a

Fig. 1 Harvard-Oxford structural brain atlas-based VOIs. Colour-coded illustration depicting the Harvard-Oxford structural brain atlas-based 3D VOIs of cortical and subcortical structures encompassing the whole brain, which were used for image analysis. Binarized masks of the 3D VOIs in orthogonal planes are shown. These binarized masks were used for extracting perfusion parameter values for various brain structures, which were subsequently used in the statistical analysis



voxel-wise approach and the resulting relative parametric measurements, i.e. MR-rCBV, MR-rCBF and C-arm CT rPBV (prefix *r*=relative), were used for the subsequent statistical analysis. Figure 2 provides an overview of these image post-processing steps. For qualitative image analysis, two readers (an experienced neuroradiologist and a trained researcher) interpreted the parametric colour-coded perfusion maps for MR-PWI and C-arm CT PBV in a blinded fashion. A consensus interpretation of the colour-coded maps was used to define the perfusion abnormalities.

Statistical analysis

Statistical analysis to explore the correlation and agreement between C-arm CT rPBV and MR-derived rCBF and rCBV parameters was performed. Pearson correlation coefficient (*r*) was calculated for (a) C-arm CT rPBV and MR-rCBV, (b) C-arm CT rPBV and MR-rCBF and (c) C-arm CT rPBV and the geometric mean of MR-rCBV and MR-rCBF ($\sqrt{\text{MR-rCBV} \times \text{MR-rCBF}}$), separately for cortical and subcortical VOIs. To assess the agreement between the two techniques, Bland-Altman analysis was employed [19]. The level of agreement was explored by plotting the difference (C-arm rPBV versus MR-rCBV; C-arm rPBV versus MR-rCBF; C-arm CT rPBV versus the geometric mean of MR-rCBV and MR-rCBF ($\sqrt{\text{MR-rCBV} \times \text{MR-rCBF}}$)) against the respective mean of the two measurements being studied, separately for both cortical and subcortical VOIs. Bias (mean difference) and 95 % limits of agreement (mean difference $\pm 1.96 \times$ standard deviation)

were calculated to assess the systematic difference and the degree of agreement, respectively.

In the next step, to explore the blood flow and blood volume weightings for C-arm CT rPBV, weighted means of MR-rCBV and MR-rCBF were calculated by assigning relative weights of 0.2, 0.4, 0.5, 0.6 and 0.8 to each parameter in a converse fashion. Bland-Altman and Pearson correlation analysis were performed for C-arm CT rPBV versus each of the calculated weighted means of MR-rCBF and MR-rCBV (rCBF 0.8+rCBV 0.2; rCBF 0.6+rCBV 0.4; rCBF 0.5+rCBV 0.5; rCBF 0.4+rCBV 0.6; rCBF 0.2+rCBV 0.8). All statistical analysis was performed using GraphPad Prism Software, San Diego, CA, USA.

Results

Study population characteristics

A total of 26 patients (mean age 55 years; men 9, women 17) entered the study. SAH on admission NCCT were graded: grade 4 in 16 (61 %), grade 3 in 9 (35 %), while one patient's NCCT head did not show evidence of SAH which was proven after lumbar puncture (4 %). The ruptured aneurysms treated by coil embolization were <5 mm in 5 (20 %), 5–10 mm in 17 (65 %) and 10–15 mm in 4 (15 %). Aneurysm locations were anterior cerebral artery, 4 (15 %); peri-callosal artery, 1 (4 %); anterior communicating artery, 7 (27 %); middle cerebral artery, 2 (8 %); posterior communicating artery, 10 (38 %); basilar artery, 1 (4 %) and internal carotid artery, 1 (4 %). Patients'

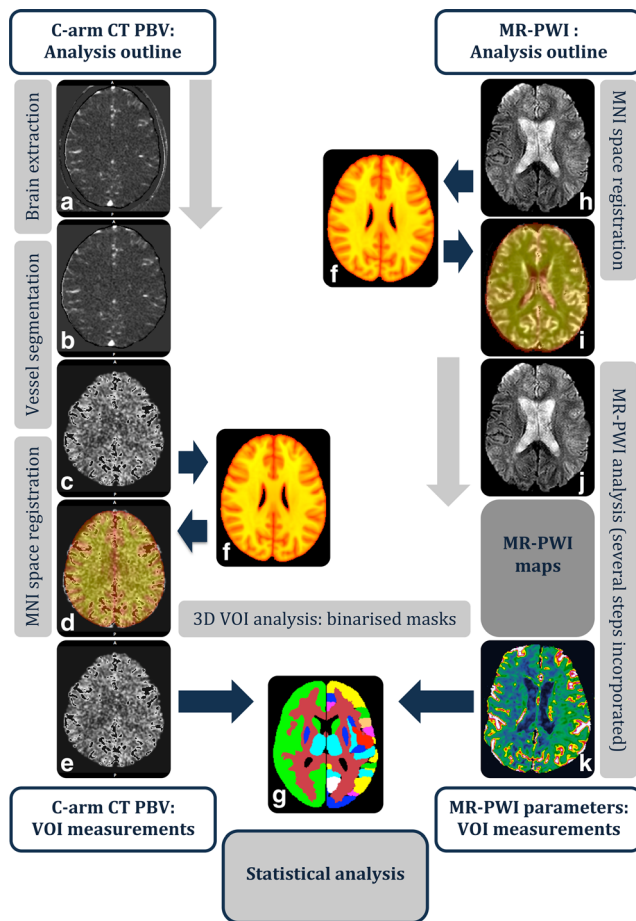


Fig. 2 A schematic overview of the image post-processing. **a** C-arm CT PBV dataset before brain extraction; **b** PBV dataset following brain extraction using FSL BET utility; **c** PBV dataset following threshold-based segmentation of the vascular structures; **d** registration of the PBV volume to the T1-weighted average structural template brain volume in MNI152 space; **e** brain-extracted, co-registered, vessel-segmented PBV volume in MNI152 space; **f** T1-weighted average structural template brain volume in MNI152 space to which the C-arm CT PBV maps and the MR-PWI data were co-registered; **g** binarized 3D-VOIs of cortical and subcortical structures encompassing the whole brain; **h** dynamic T2* weighted MR-PWI dataset; **i** registration of the MR-PWI to T1-weighted average structural template brain volume in MNI152 space; **j** registered MR-PWI dataset which was subsequently post-processed to extract perfusion parametric maps preserving the spatial coordinates in MNI152 space; **k** motion-corrected, vessel-segmented, brain-extracted, leakage-corrected, registered MR-PWI maps. Subsequently, using the binarized 3D-VOIs, the perfusion parametric values were obtained for the cortical and subcortical structures, which were then used in the statistical analysis

WFNS (world federation of neurosurgical societies) grades at the time of admission to hospital were grade 1 in 16 (61 %), grade 2 in 7 (27 %), grade 3 in 2 (8 %) and grade 4 in 1 patient (4 %). The onset of clinical deterioration after SAH varied from day 2 post-SAH to day 12 post-SAH (median, day 7 post-SAH).

After the diagnosis of DCI, all patients received standard medical management by the multidisciplinary neuro-ICU team according to the institutional protocol, with no change

in treatment between the two study scans (MR-PWI and C-arm CT PBV). Physiological parameters were recorded for each patient, and stability between the scans was ensured. Mean duration between the C-arm FDCT PBV scan and the MR imaging was 124 min. Using the colour-coded parametric maps, MR perfusion abnormalities (focal perfusion deficits or asymmetric hemispheric perfusion) were diagnosed in 23 patients (88 %) as evidenced by decreased CBF, decreased CBV or prolonged MTT. C-arm CT correctly identified 21 of the 23 patients with MR perfusion abnormalities (sensitivity relative to MR-PWI, 0.91). The 3 patients with normal MR perfusion distribution were correctly interpreted to have normal C-arm PBV maps (specificity relative to MR-PWI, 1.0). Of the 26 patients, 8 (31 %) underwent chemical angioplasty with selective intra-arterial nimodipine administration, of whom 2 (8 %) received chemical angioplasty treatment twice. Catheter angiogram findings in conjunction with the clinical/neurological status of patients were used as the primary criteria by the treating interventional neuroradiologist to determine if chemical angioplasty would be beneficial to the patient. The patient characteristics are summarized in Table 1.

Quantitative image analysis

- (a) The Bland-Altman analysis demonstrated good agreement between the C-arm CT rPBV and the MR-rCBV and rCBF measurements, both for cortical and subcortical VOIs. In its comparison against MR-rCBV and rCBF, there was minimal bias in the C-arm CT rPBV measurements (C-arm CT rPBV vs MR-rCBF, 0.022 ± 0.17 and 0.062 ± 0.17 ; C-arm CT rPBV vs MR-rCBV, 0.036 ± 0.20 and 0.032 ± 0.24 , for cortical and subcortical VOIs, respectively). The width of interval between the 95 % limits of agreement was relatively narrower for C-arm CT rPBV vs MR-rCBF (-0.31 to 0.35 and -0.32 to 0.44 , for cortical and subcortical VOIs, respectively) compared with C-arm CT rPBV vs MR-rCBV (-0.39 to 0.46 and -0.47 to 0.53 , for cortical and subcortical VOIs, respectively), indicating better agreement for C-arm CT rPBV vs MR-rCBF. The C-arm CT rPBV measurements showed good correlation with both MR-rCBV and MR-rCBF, which were statistically significant ($p < 0.001$). The correlation was slightly stronger for C-arm CT rPBV vs MR-rCBF ($r = 0.85$ and 0.78) compared with C-arm CT rPBV vs MR-rCBV ($r = 0.72$ and 0.69). Overall, the techniques correlated better for cortical VOIs compared with the subcortical VOIs.
- (b) Given the slightly better correlation and stronger agreement of C-arm CT rPBV with MR-rCBF compared with MR-rCBV, which suggested that C-arm CT rPBV may have weightings of both rCBV and rCBF, the geometric mean of MR-rCBV and MR-rCBF ($\sqrt{\text{MR-rCBV} \times \text{MR-rCBF}}$) was calculated; the correlation and agreement

Table 1 Demographics, clinical characteristics and imaging and treatment details for the recruited patients

Patient number	Age (years)	Gender (M/F)	Aneurysm location	Aneurysm size (mm)	WFNS grade	Fischer grade	DCI onset (day) ^a	MR-PWI deficits	PBV deficits	Medical management	Angioplasty
1	47	M	Anterior communicating artery	6×4	1	3	6	+	+	+	+
2	55	F	Left anterior cerebral artery	12×10	3	4	10	+	+	+	-
3	61	F	Right posterior communicating artery	8×5	2	3	9	+	+	+	-
4	49	F	Anterior communicating artery	10×7	1	3	4	+	+	+	-
5	68	F	Right posterior communicating artery	10×6	2	4	8	+	+	+	-
6	71	F	Anterior communicating artery	6×5	1	4	4	+	+	+	+
7	46	M	Right middle cerebral artery	4×3	3	3	6	+	+	+	++
8	77	F	Left anterior cerebral artery	6×4	1	4	4	+	+	+	-
9	46	M	Right posterior communicating artery	4×4	1	4	9	+	+	+	-
10	50	F	Right internal carotid artery	3×3	1	3	2	+	+	+	-
11	53	F	Basilar artery tip	7×6	2	3	5	+	+	+	+
12	55	M	Right posterior communicating artery	5×3	2	4	12	+	+	+	-
13	55	F	Left posterior communicating artery	4×4	2	4	7	+	+	+	-
14	69	F	Left anterior cerebral artery	11×7	1	4	2	+	+	+	+
15	66	M	Anterior communicating artery	7×5	1	0 ^b	10	+	+	+	-
16	45	M	Anterior communicating artery	15×8	2	4	8	+	+	+	+
17	66	M	Right middle cerebral artery	8×3	4	4	7	+	+	+	+
18	30	M	Anterior communicating artery	7×4	1	3	9	+	+	+	-
19	39	F	Right posterior communicating artery	5×3.5	1	4	11	+	+	+	++
20	50	F	Anterior communicating artery	4×3.5	1	4	5	+	+	+	-
21	69	M	Right posterior communicating artery	7×4	1	4	6	-	-	+	-
22	39	F	Right posterior communicating artery	10×9	1	4	5	-	-	+	-
23	52	F	Right posterior communicating artery	5×5	1	4	7	+	+	+	-
24	54	F	Left posterior communicating artery	8×5	1	3	8	+	+	+	-
25	58	F	Right anterior cerebral artery	5×4	1	3	5	-	-	+	-
26	60	F	Left peri-callosal artery	12×8	2	4	5	+	+	+	-

^a DCI onset—clinical deterioration occurring on 'n'th day after aneurysmal SAH^b NCCT head was negative for SAH, which was later confirmed on lumbar puncture

analysis were then performed for C-arm CT rPBV versus the geometric mean of MR-rCBV and MR-rCBF. There was improved agreement and better correlation of C-arm CBT rPBV with the geometric mean of MR-rCBV and MR-rCBF ($\sqrt{\text{MR-rCBV} \times \text{MR-rCBF}}$), compared with MR-rCBV or MR-rCBF alone (calculated in the first step). For C-arm CT rPBV vs $\sqrt{\text{MR-rCBV} \times \text{MR-rCBF}}$, results of agreement and correlation analysis were: bias 0.018 ± 0.13 and 0.042 ± 0.13 , 95 % limits of agreement -0.25 to 0.29 and -0.28 to 0.36 , and Pearson correlation coefficient (r) 0.89 (95 % CI 0.86 to 0.91) and 0.86 (95 % CI 0.83 to 0.89), for cortical and subcortical VOIs, respectively.

- (c) To explore the relative weightings of MR-rCBV and rCBF for C-arm CT rPBV, weighted means of MR-rCBV and rCBF were calculated by assigning relative weights of 0.2, 0.4, 0.5, 0.6 and 0.8 to MR-rCBV and rCBF in a converse fashion; the agreement and correlation analyses were then performed for each of the calculated weighted means. MR-rCBF 0.6+MR-rCBV 0.4 (i.e. 60 % rCBF and 40 % rCBV) showed best agreement and correlation with C-arm CT rPBV (Bland-Altman analysis: bias 0.015 ± 0.119 and 0.043 ± 0.118 , 95 % limits of agreement -0.21 to 0.24 and -0.23 to 0.31 and Pearson correlation coefficient (r) 0.91 (95 % CI 0.89 to 0.93) and 0.88 (95 % CI 0.85 to 0.90), for cortical and subcortical VOIs, respectively). The results of Bland-Altman analysis and the Pearson correlation analysis are summarized in Tables 2 and 3 and are depicted in Figs. 3, 4 and 5. Illustrative case examples are presented in Figs. 6 and 7.

deterioration. We observed good correlation and agreement between the C-arm CT rPBV and MR-PWI-derived rCBV and rCBF, with minimal bias and the 95 % limits of agreement that included clinically significant rPBV discrepancies. Our results demonstrate that the C-arm CT PBV is a composite parameter with both blood flow and blood volume weightings (better correlation and agreement of C-arm CT rPBV with the geometric mean of MR-rCBV and MR-rCBF ($\sqrt{\text{MR-rCBV} \times \text{MR-rCBF}}$) compared with MR-rCBV or MR-rCBF alone). Furthermore, the C-arm CT PBV has a preferential blood flow weighting (≈ 60 % blood flow and ≈ 40 % blood volume weighting) as shown by the results of analysis performed using the weighted means of MR-rCBF and rCBV (Tables 2 and 3).

In comparing the C-arm CT PBV with the MR-PWI-derived parameters, we focused on a quantitative analysis approach using predefined atlas-based cortical and subcortical VOIs encompassing the whole brain. The comprehensive set of VOIs (56 VOIs for each hemisphere) that we used included all cortical and subcortical structures as depicted in Fig. 1. Robust registration between the two datasets for each patient was performed to ensure that the VOIs being compared corresponded to the same anatomical locations in the brain. This approach makes our comparison objective and minimizes any observer bias that may be introduced if manually drawn 2D regions of interest (ROIs) were used. With limited number of 2D ROIs, used in the initial studies comparing C-arm CT PBV with CTP-CBV where a limited brain volume coverage was available for CTP, there remains a possibility that certain locations of brain with perfusion deficits may be partially or completely excluded [12, 13, 20]. In addition, with limited brain coverage for CTP, its co-registration with another study is invariably inadequate and any differences in slice orientation can lead to anatomical non-correspondence between the images being compared. With both C-arm CT imaging and MR-PWI, there is extended craniocaudal (z -axis) coverage; therefore, co-registration of the two studies to

Discussion

This study demonstrates the feasibility and potential value of intravenous PBV protocol C-arm FDCT imaging in patients with aneurysmal SAH who develop delayed clinical

Table 2 Results of Bland-Altman analysis of agreement and Pearson correlation analysis

	Bland-Altman analysis			Pearson correlation analysis			
	Bias	SD of bias	95 % limits of agreement	r	95 % CI	R-square	p value
Cortical VOIs							
C-arm CT rPBV vs MR-rCBF	0.022	0.17	-0.31 to 0.35	0.85	0.83 to 0.86	0.71	<0.001
C-arm CT rPBV vs MR-rCBV	0.036	0.20	-0.39 to 0.46	0.72	0.69 to 0.75	0.52	<0.001
C-arm CT rPBV vs $\sqrt{(\text{MR-rCBV} \times \text{MR-rCBF})}$	0.018	0.13	-0.25 to 0.29	0.89	0.86 to 0.91	0.75	<0.001
Subcortical VOIs							
C-arm CT rPBV vs MR-rCBF	0.062	0.17	-0.32 to 0.44	0.78	0.73 to 0.82	0.61	<0.001
C-arm CT rPBV vs MR-rCBV	0.032	0.24	-0.47 to 0.53	0.69	0.62 to 0.75	0.47	<0.001
C-arm CT rPBV vs $\sqrt{(\text{MR-rCBV} \times \text{MR-rCBF})}$	0.042	0.13	-0.28 to 0.36	0.86	0.83 to 0.89	0.69	<0.001

Table 3 Results of Bland-Altman agreement and Pearson correlation analyses for weighted MR-rCBF and rCBV

C-arm CT rPBV vs	Bland-Altman analysis			Pearson correlation analysis			
	Bias	SD of bias	95 % limits of agreement	<i>r</i>	95 % CI	R-square	<i>p</i> value
Cortical VOIs							
MR-rCBF 0.8+MR-rCBV 0.2	0.019	0.148	−0.26 to 0.30	0.88	0.85 to 0.90	0.76	<0.001
MR-rCBF 0.6+MR-rCBV 0.4	0.015	0.119	−0.21 to 0.24	0.91	0.89 to 0.93	0.81	<0.001
MR-rCBF 0.5+MR-rCBV 0.5	0.018	0.127	−0.24 to 0.28	0.84	0.81 to 0.88	0.76	<0.001
MR-rCBF 0.4+MR-rCBV 0.6	0.023	0.133	−0.27 to 0.31	0.80	0.77 to 0.84	0.71	<0.001
MR-rCBF 0.2+MR-rCBV 0.8	0.031	0.163	−0.33 to 0.39	0.77	0.73 to 0.81	0.62	<0.001
$\sqrt{(\text{MR-rCBF} \times \text{MR-rCBV})}$	0.018	0.132	−0.25 to 0.29	0.89	0.86 to 0.91	0.77	<0.001
Subcortical VOIs							
MR-rCBF 0.8+MR-rCBV 0.2	0.052	0.127	−0.27 to 0.37	0.83	0.79 to 0.86	0.68	<0.001
MR-rCBF 0.6+MR-rCBV 0.4	0.043	0.118	−0.23 to 0.31	0.88	0.85 to 0.90	0.75	<0.001
MR-rCBF 0.5+MR-rCBV 0.5	0.041	0.139	−0.26 to 0.34	0.84	0.81 to 0.87	0.70	<0.001
MR-rCBF 0.4+MR-rCBV 0.6	0.037	0.171	−0.30 to 0.37	0.79	0.76 to 0.83	0.64	<0.001
MR-rCBF 0.2+MR-rCBV 0.8	0.034	0.219	−0.39 to 0.45	0.76	0.71 to 0.80	0.56	<0.001
$\sqrt{(\text{MR-rCBF} \times \text{MR-rCBV})}$	0.042	0.129	−0.28 to 0.36	0.86	0.83 to 0.89	0.69	<0.001

achieve anatomical correspondence is convenient, and in conjunction with the VOIs including all brain regions, this approach ensures that no parts of the brain are excluded from the analysis and that the VOIs being compared represent the same regions of brain for the two imaging studies. We acknowledge that the perfusion deficits in DCI may not follow the exact anatomical boundaries of atlas-based VOIs, but

using a combination of robust registration and whole brain VOIs makes the comparisons valid by virtue of anatomical correspondence and whole brain inclusion, irrespective of the distribution of perfusion abnormalities.

Previous reports documenting the accuracy of C-arm CT PBV technique in both animal and human subjects used CTP as a comparison standard and restricted their analysis to

Fig. 3 Agreement and correlation analysis plots for C-arm CT rPBV versus MR-PWI rCBV. Bland-Altman plots of agreement (a, c) and Pearson correlation plots (b, d) of C-arm CT rPBV versus MR-PWI rCBV for cortical (a, b) and subcortical (c, d) VOIs, respectively

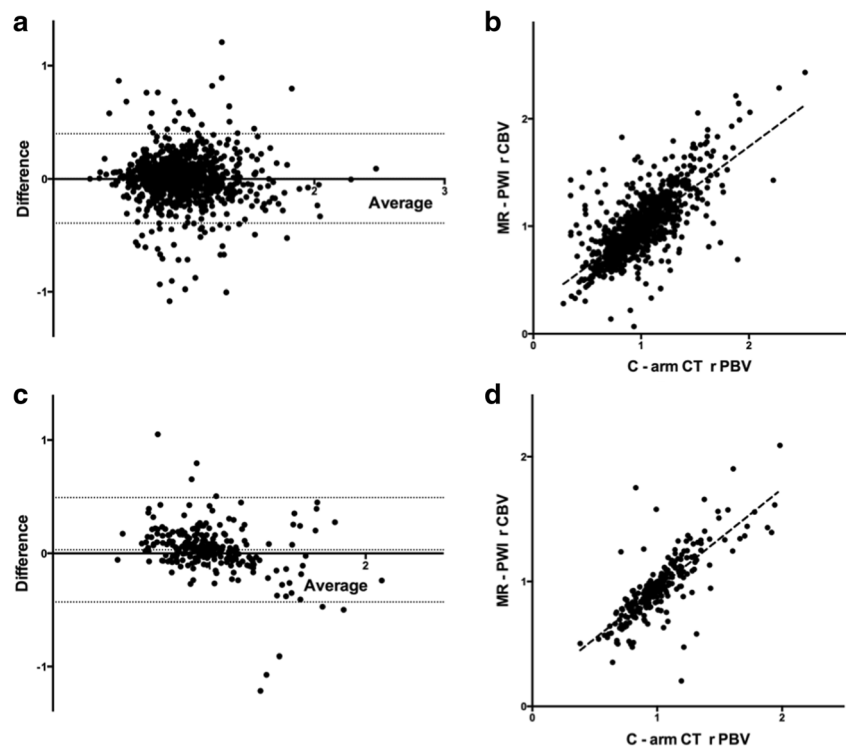
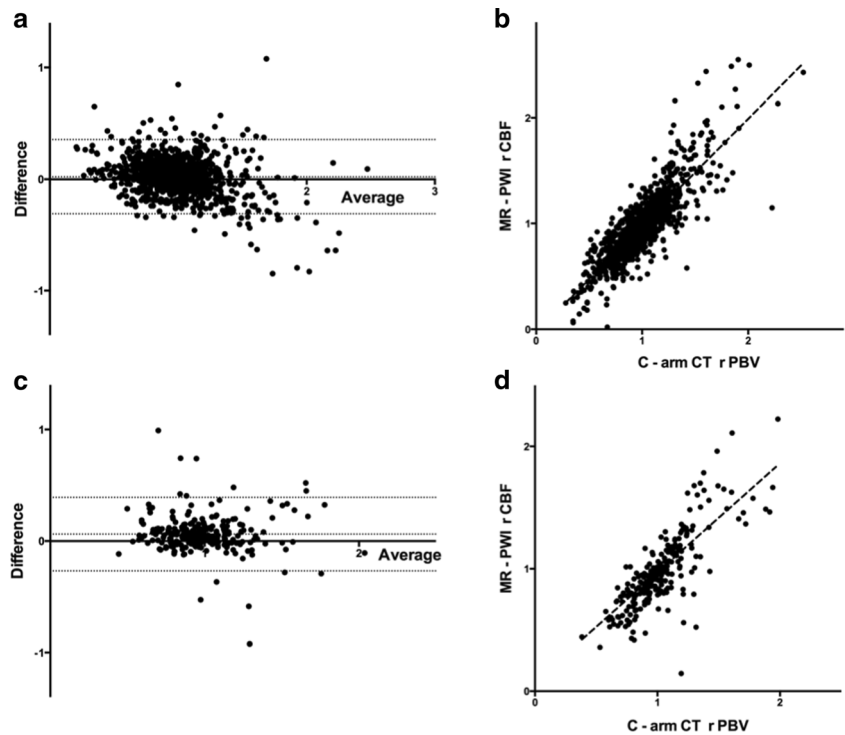


Fig. 4 Agreement and correlation analysis plots for C-arm CT rPBV versus MR-PWI rCBF. Bland-Altman plots of agreement (a, c) and Pearson correlation plots (b, d) for C-arm CT PBV versus MR-PWI rCBF for cortical (a, b) and subcortical (c, d) VOIs, respectively



comparison of PBV with CBV measurements only [2–5, 21]. A comparison of C-arm CT PBV against CTP-CBV alone makes an a priori assumption regarding equivalence of C-arm CT PBV and CTP-CBV, which is not completely

unjustified based on the theoretical understanding [1]. Our observations support the findings of previous reports in confirming the agreement between CBV and C-arm CT PBV by using a different perfusion imaging modality, i.e. MR-PWI.

Fig. 5 Agreement and correlation analysis plots for C-arm CT rPBV versus weighted mean of MR-PWI rCBV and rCBF. Bland-Altman plots of agreement (a, c) and Pearson correlation plots (b, d) for C-arm CT PBV versus weighted mean of MR-PWI rCBV and rCBF (rCBF 0.6, rCBV 0.4) for cortical (a, b) and subcortical (c, d) VOIs, respectively

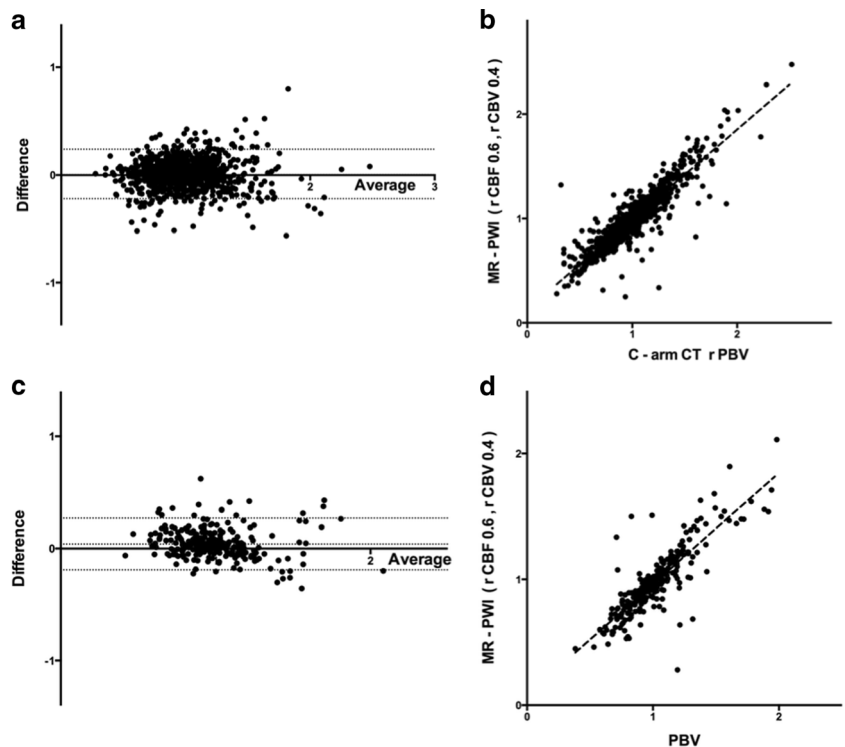
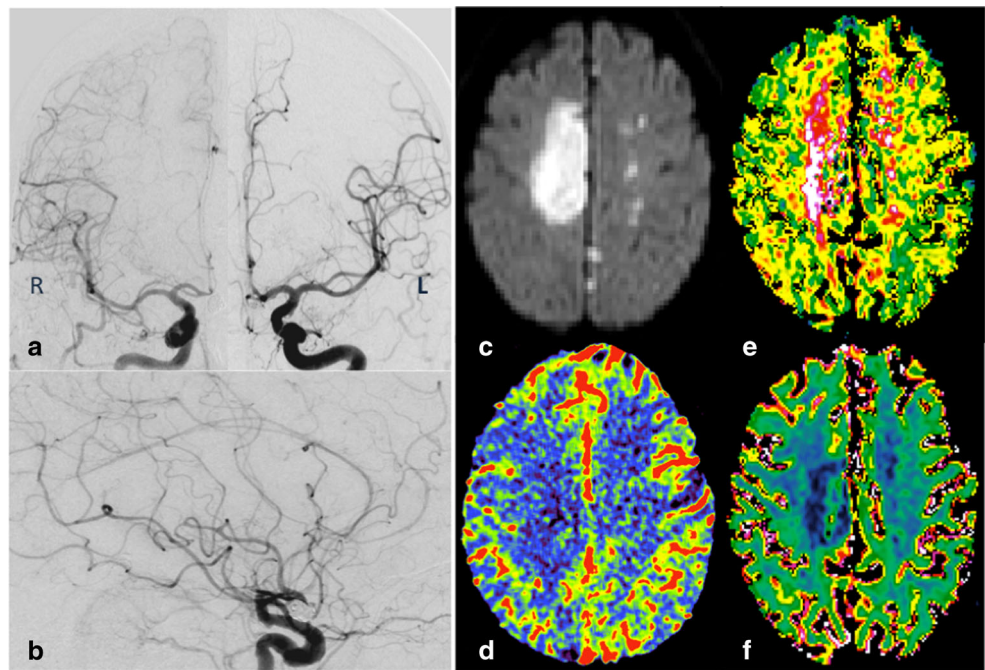


Fig. 6 Illustrative case example 1. A 50-year-old-woman with ruptured anterior communicating artery aneurysm developing left hemiparesis on day 6 post-SAH: Catheter angiogram images (**a, b**) show intense vasospasm affecting both ACAs (right>left) with corresponding abnormality (restricted diffusion) on MR-DWI image indicating established infarcts in the same territory (**c**). C-arm CT PBV (**d**), MR-PWI rMTT (**e**) and MR-PWI rCBV (**f**) images show asymmetric parametric deficits in the same distribution



However, exploratory nature of analysis in this paper comparing C-arm CT rPBV against both MR-PWI rCBV and rCBF, with no a priori assumption regarding equivalence of PBV and CBV provides additional insight into the composite nature of C-arm CT PBV parameter. We noticed a slightly higher correlation and better agreement of C-arm CT rPBV with MR-

rCBF in comparison with MR-rCBV. Subsequent analysis using the geometric mean of MR-rCBV and MR-rCBF ($\sqrt{MR-rCBV \times MR-rCBF}$), which showed better correlation and agreement with C-arm CT PBV, compared with MR-rCBV or MR-rCBF alone, provided support to the proposition that C-arm CT PBV is a composite perfusion parameter, distinct from

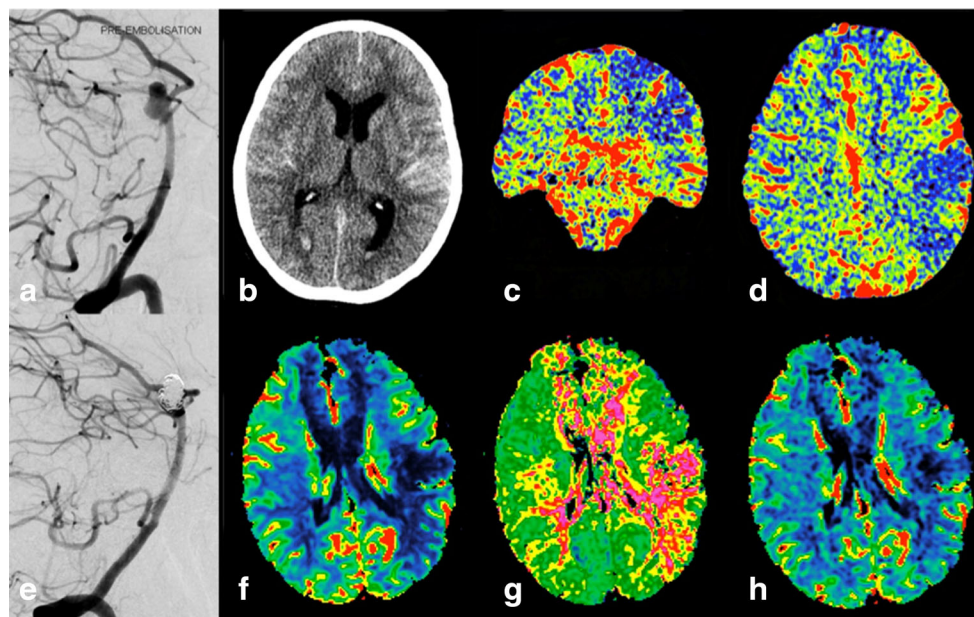


Fig. 7 Illustrative case example 2. A 52-year-old-woman with ruptured basilar artery termination aneurysm **a** pre-treatment and **e** post-treatment catheter angiogram images show coil embolization and complete angiographic occlusion of the basilar artery termination aneurysm; **b** NCCT performed after the development of neurological deficits (day 4)

excludes rebleed, hydrocephalus or infarction; **c, d** coronal and axial sections of C-arm FDCT PBV maps (day 6) show reduced PBV in both frontal lobes and in the left parietal lobe and **f–h** MR-PWI CBF, MTT and CBV maps (day 6) confirming a similar distribution of reduced perfusion in both frontal lobes and in the left parietal lobe

CBV, and likely has both CBV and CBF weightings. With further analysis using weighted means of MR-rCBF and rCBV, we were able to demonstrate that C-arm CT PBV has approximately 60 % blood flow and 40 % blood volume weighting. These objective findings also corresponded with our subjective observations in the clinical setting where the deficits on colour-coded PBV maps were noted to visually correlate better with the pattern of abnormality on MR-CBF maps than with the pattern of abnormality on MR-CBV maps. None of the prior studies have explored this subject for C-arm CT PBV. However, our results are supported by similar findings for multi-detector CT (MDCT). The image data acquired by C-arm CT PBV protocol is post-processed using the principles of image subtraction and indicator dilution in a manner similar to that proposed initially for multi-detector CT/CTA PBV imaging [6]. For MDCT, the CTA source images (SI) could be used alone or could be post-processed to generate colour-coded MDCT PBV maps [7–9]. Sharma et al., using a CTA protocol with a scan duration and contrast injection parameters comparable to our C-arm CT PBV examination, showed that despite theoretical models suggesting MDCT PBV images to be predominately blood volume weighted, with more rapid modern CTA protocols used in clinical practice, these images were in fact blood flow weighted [10]. In this setting, blood volume weighting is facilitated by (a) longer delay and lower contrast injection rates to change the temporal shape of the time-concentration curve or (b) by longer scanning times to acquire data over a larger segment of the time-concentration-curve, while the converse factors favour blood flow weighting [22]. Furthermore, keeping in view the altered cerebrovascular haemodynamics in the setting of DCI (our study population), with vessel narrowing and subsequent increased intracranial vascular resistance, the passage of intravenously administered contrast medium through the cerebral vasculature could have been delayed resulting in the C-arm FDCT projections being acquired while the contrast concentration in the cerebral microvasculature may still have been rising, thus providing another contributory factor to preferential blood flow weighting of the resulting C-arm CT PBV measurements.

We did not use ‘presence of infarcts on the follow-up imaging’, as a criterion to define DCI. The absence of infarcts on follow-up imaging does not completely exclude prior DCI since the cerebral ischemia could have been transient and the infarction prevented by spontaneous resolution or by successful treatment (all patients enrolled in our study received medical management, while some underwent chemical angioplasty) [13]. Thus, using a follow-up imaging criterion to retrospectively define DCI can potentially underestimate the occurrence of DCI. Instead, the patients recruited for this research were initially labelled to have DCI on the basis of clinical criteria (described in ‘Materials and methods’). Confirmation of the clinically labelled DCI using MR imaging

imposed logistical constraints for neuro-ICU patients particularly related to the *continuous monitoring equipment* that these very sick patients required. These constraints were less challenging for C-arm FDCT scanning due to a more open and non-magnetic environment.

The C-arm CT PBV technique is new, and there are no established guidelines regarding its incorporation in the workflow for management of DCI patients. We anticipate that the information provided by whole brain PBV measurements in an interventional setting can be of potential benefit in a subset of aneurysmal SAH patients, for example, (a) a C-arm CT PBV scan at the time of initial embolization treatment may serve as a baseline for critically ill patients with large volume SAH (high Fischer grade) considered at high risk for developing DCI and (b) in patients developing DCI with no improvement in their neurological status despite aggressive medical management, who undergo catheter angiogram to evaluate the degree of angiographic vasospasm, a C-arm CT PBV study may either provide useful supplemental information on the hemodynamic significance of angiographic large vessel vasospasm or help to identify the microvascular dysfunction which may not be detectable on the 2D-DSA. For these patients, PBV abnormalities, when present, may have a predictive value for DCI similar to CTP parameters and help plan a rescue intervention without the need for patient transfer between the diagnostic and interventional suites. This study demonstrates the feasibility of C-arm CT PBV imaging in the setting of DCI following aneurysmal SAH and its agreement with MR-PWI; however, future studies investigating the correlation of C-arm CT PBV deficits to the development of infarction on follow-up imaging and larger studies specifically exploring its utility in the diagnosis and management of DCI would be needed to elucidate its true clinical value.

Apart from the major advantage of its availability in the interventional suite, C-arm CT PBV protocol imaging offers additional features including (a) an extended craniocaudal coverage that allows whole brain evaluation in a single sweep, (b) isotropic spatial resolution that makes omniplane reconstructions of the C-arm CT PBV maps possible (both a and b may not synchronously be available for CTP and MR-PWI), (c) large vessel angiographic reconstructions from the data collected during contrast-enhanced run of the C-arm CT PBV protocol scan and (d) cross-sectional CT-like soft tissue reconstructions of the brain parenchyma from the data collected during the mask run. The large vessel reconstructions can reliably evaluate the patency and calibre of large intracranial arteries for the presence of an occlusion or vasospasm, while the soft tissue reconstructions, despite their inferior low-contrast resolution compared with conventional CT, are of adequate quality to allow assessment of ventricular size, intracranial haemorrhage and procedural vessel rupture [23]. Thus, a single intravenous PBV protocol C-arm CT examination provides soft tissue, angiographic and haemodynamic

information, obtaining which may otherwise require multiple imaging studies thereby avoiding repeat examinations and reducing the overall radiographic contrast and radiation doses. The ability to extract diagnostic anatomical and physiological data in an interventional environment has potential implications for management of patients with ischemic cerebrovascular disease. In the setting of acute stroke, for example, a single C-arm CT study can help exclude intracranial haemorrhage, assess large vessel patency and estimate tissue viability, thereby assisting in patient selection for endovascular revascularization treatment without the need to transfer patients to a CT or MR scanner. A reduction in the duration between the patients' arrival at a stroke treatment facility and start of revascularization procedure thus achieved could increase the likelihood of improved procedural and clinical outcomes. Additionally, by virtue of its availability in the interventional suite, it can help optimize and assess the success of revascularization procedures in restoring perfusion while the patient is still on angio-table.

We used MR-PWI as a reference standard, while the previous studies have used CTP as the comparison standard for C-arm CT PBV evaluation [2–5, 21, 24]. CTP offers obvious advantages including widespread availability, easier logistics, absolute quantification of perfusion parameters and relatively few contraindications. However, its limited craniocaudal coverage may be restrictive in the setting of DCI, where the ischemic changes could be multifocal or global in nature [12–14, 25]. Our choice of MR-PWI as a reference standard was thus driven partly by its extended craniocaudal coverage but largely by the lack of radiation exposure with MR imaging, with an aim to limit radiation dose for the critically ill study subjects undergoing a research scan that involved radiation exposure and who typically underwent multiple x-ray-based diagnostic imaging studies. Another advantage of choosing MR imaging was the availability of diffusion-weighted images from the same scanning session, which are sensitive to detect early cytotoxic oedema and infarction (88–100 % sensitivity to detect early infarcts) [26]. However, both MR-PWI and CTP are well established and validated perfusion imaging techniques, routinely used in clinical practice. A disadvantage of MR-PWI-derived perfusion parameters is their semi-quantitative nature due to the lack of a direct linear relationship between the MR signal intensity and the paramagnetic contrast medium concentration [27]. We recognized this limitation, and in our analysis, we used the interhemispheric ratios of the perfusion parameters for both the MR-PWI and C-arm CT techniques. While it is theoretically possible that in multifocal or diffuse ischemia where symmetric perfusion deficits exist, the interhemispheric ratios may be misleading. However, an advantage of C-arm CT PBV imaging is that absolute PBV measurements (given the use of iodinated contrast and x-rays) are also provided, and in the setting of multifocal or diffuse ischemia, these absolute

measurements provide information that may be overlooked if only the interhemispheric ratios were used.

Although measurement of a physiological parameter (PBV) of potential prognostic significance is an important step towards functional imaging in the neurointerventional suite, mechanical constraints prevent dynamic perfusion imaging with the C-arm systems [4]. At the current level of performance, thus C-arm CT PBV imaging remains inferior to the conventional dynamic perfusion imaging modalities and should not be considered to replace CTP or MR-PWI; rather it serves as an additional tool in the neurointerventionist's armamentarium. In evaluating its value as a clinical imaging tool, therefore, the application-related advantages given its availability in interventional setting should be weighed against the image performance-related disadvantages. New generation multi-axis C-arm angiographic systems based on robotic technology allow shorter rotation times and hold the potential for dynamic perfusion imaging. Preliminary work in canines based on interleaved scanning to augment the temporal resolution for C-arm systems has shown promising results in allowing estimation of CBF and MTT [28, 29]. Further advancements such as improved flat detector contrast detectability and read-out speed, improvements in C-arm system design and newer software algorithms are expected to support this development, which would allow a detailed 'one-stop' assessment of patients with cerebral ischemia in the neurointerventional suite.

Conclusion

In conclusion, the work in this paper provides insight into the nature of C-arm CT PBV parameter and demonstrates the feasibility of C-arm CT PBV imaging in the setting of DCI following aneurysmal SAH. In this first report on the application of C-arm CT PBV imaging in patients with DCI and its comparison with MR-PWI, we demonstrate that C-arm CT PBV is a composite perfusion parameter incorporating both blood flow and blood volume weightings. That PBV has preferential (60 %) blood flow weighting is an important finding with potential clinical significance, particularly when interpreting the C-arm CT PBV maps in the setting of acute brain ischemia, where an assumed CBV equivalence can potentially overestimate the infarcted tissue and lead to selection of fewer patients for endovascular treatment. In this regard, for the purpose of clarity, we recommend that the term parenchymal blood volume (PBV) be preferred and the term cerebral blood volume (CBV) be avoided when referring to this hemodynamic parameter measured using steady-state C-arm CT imaging. As a non-invasive objective assessment tool, the ability of a single C-arm CT study to provide both anatomical (soft tissue and angiographic) and physiological information in the interventional suite improves the workflow, can avoid repeat examinations, serve as a diagnostic marker for DCI,

potentially allow in-room selection of patients for intra-arterial angiography and angioplasty, and has implications for management of patients with acute stroke.

Acknowledgments The authors would like to thank the staff and Department of Neuroradiology, John Radcliffe Hospital, Oxford, UK, for their support in patient recruitment and scanning. We also thank Siemens for the hardware and software support. MK would like to thank The Rhodes Trust, Oxford, for funding his doctoral studies at the University of Oxford.

Ethical Standards and Patient Consent We declare that all human and animal studies have been approved by the Coventry Research Ethics Committee and have therefore been performed in accordance with the ethical standards laid down in the 1964 Declaration of Helsinki and its later amendments. We declare that all patients gave informed consent prior to inclusion in this study.

Conflict of Interest We declare that we have no conflict of interest.

References

- Zellerhoff M, Deuerling-Zheng Y, Strother CM, et al (2009) Measurement of cerebral blood volume using angiographic C-arm systems. p 72620H–72620H–8
- Ahmed AS, Zellerhoff M, Strother CM et al (2009) C-Arm CT measurement of cerebral blood volume: an experimental study in canines. *Am J Neuroradiol* 30:917–922. doi:10.3174/ajnr.A1513
- Bley T, Strother CM, Pulfer K et al (2010) C-Arm CT measurement of cerebral blood volume in ischemic stroke: an experimental study in canines. *Am J Neuroradiol* 31:536–540. doi:10.3174/ajnr.A1851
- Struffert T, Deuerling-Zheng Y, Engelhorn T et al (2012) Feasibility of cerebral blood volume mapping by flat panel detector CT in the angiography suite: first experience in patients with acute middle cerebral artery occlusions. *Am J Neuroradiol* 33:618–625. doi:10.3174/ajnr.A2839
- Struffert T, Deuerling-Zheng Y, Kloska S et al (2011) Cerebral blood volume imaging by flat detector computed tomography in comparison to conventional multislice perfusion CT. *Eur Radiol* 21:882–889. doi:10.1007/s00330-010-1957-6
- Hamberg LM, Hunter GJ, Kierstead D et al (1996) Measurement of cerebral blood volume with subtraction three-dimensional functional CT. *Am J Neuroradiol* 17:1861–1869
- Wittkamp G, Buerke B, Dziejewski R et al (2010) Whole brain perfused blood volume CT: visualization of infarcted tissue compared to quantitative perfusion CT. *Acad Radiol* 17:427–432. doi:10.1016/j.acra.2009.11.005
- Lu J, Zhang M, Cao Y et al (2011) Three-dimensional whole-brain perfused blood volume imaging with multimodal CT for evaluation of acute ischaemic stroke. *Clin Radiol* 66:517–525. doi:10.1016/j.crad.2011.01.003
- Kloska SP, Fischer T, Nabavi DG et al (2007) Color-coded perfused blood volume imaging using multidetector CT: initial results of whole-brain perfusion analysis in acute cerebral ischemia. *Eur Radiol* 17:2352–2358. doi:10.1007/s00330-007-0580-7
- Sharma M, Fox AJ, Symons S et al (2011) CT angiographic source images: flow- or volume-weighted? *Am J Neuroradiol* 32:359–364. doi:10.3174/ajnr.A2282
- Diringer MN, Bleck TP, Claude Hemphill J 3rd et al (2011) Critical care management of patients following aneurysmal subarachnoid hemorrhage: recommendations from the Neurocritical Care Society's Multidisciplinary Consensus Conference. *Neurocrit Care* 15:211–240. doi:10.1007/s12028-011-9605-9
- Dankbaar JW, Rijdsdijk M, van der Schaaf IC et al (2009) Relationship between vasospasm, cerebral perfusion, and delayed cerebral ischemia after aneurysmal subarachnoid hemorrhage. *Neuroradiology* 51:813–819. doi:10.1007/s00234-009-0575-y
- Dankbaar JW, de Rooij NK, Rijdsdijk M et al (2010) Diagnostic threshold values of cerebral perfusion measured with computed tomography for delayed cerebral ischemia after aneurysmal subarachnoid hemorrhage. *Stroke* 41:1927–1932. doi:10.1161/STROKEAHA.109.574392
- Sanelli PC, Ugorec I, Johnson CE et al (2011) Using quantitative CT perfusion for evaluation of delayed cerebral ischemia following aneurysmal subarachnoid hemorrhage. *Am J Neuroradiol* 32:2047–2053. doi:10.3174/ajnr.A2693
- Fisher CM, Kistler JP, Davis JM (1980) Relation of cerebral vasospasm to subarachnoid hemorrhage visualized by computerized tomographic scanning. *Neurosurgery* 6:1–9
- Jenkinson M, Beckmann CF, Behrens TEJ et al (2012) FSL. *NeuroImage* 62:782–790. doi:10.1016/j.neuroimage.2011.09.015
- Smith SM (2002) Fast robust automated brain extraction. *Hum Brain Mapp* 17:143–155. doi:10.1002/hbm.10062
- Jenkinson M, Bannister P, Brady M, Smith S (2002) Improved optimization for the robust and accurate linear registration and motion correction of brain images. *NeuroImage* 17:825–841
- Martin Bland J, Altman D (1986) Statistical methods for assessing agreement between two methods of clinical measurement. *Lancet* 327:307–310. doi:10.1016/S0140-6736(86)90837-8
- Rijdsdijk M, van der Schaaf IC, Velthuis BK et al (2008) Global and focal cerebral perfusion after aneurysmal subarachnoid hemorrhage in relation with delayed cerebral ischemia. *Neuroradiology* 50:813–820. doi:10.1007/s00234-008-0416-4
- Struffert T, Deuerling-Zheng Y, Kloska S et al (2010) Flat detector CT in the evaluation of brain parenchyma, intracranial vasculature, and cerebral blood volume: a pilot study in patients with acute symptoms of cerebral ischemia. *Am J Neuroradiol* 31:1462–1469. doi:10.3174/ajnr.A2083
- Konstas AA, Goldmakher GV, Lee T-Y, Lev MH (2009) Theoretic basis and technical implementations of CT perfusion in acute ischemic stroke, part 1: theoretic basis. *Am J Neuroradiol* 30:662–668. doi:10.3174/ajnr.A1487
- Kamran M, Nagaraja S, Byrne JV (2010) C-arm flat detector computed tomography: the technique and its applications in interventional neuro-radiology. *Neuroradiology* 52:319–327. doi:10.1007/s00234-009-0609-5
- Mordasini P, El-Koussy M, Brekenfeld C et al (2012) Applicability of tableside flat panel detector CT parenchymal cerebral blood volume measurement in neurovascular interventions: preliminary clinical experience. *Am J Neuroradiol* 33:154–158. doi:10.3174/ajnr.A2715
- Mir DIA, Gupta A, Dunning A et al (2013) CT perfusion for detection of delayed cerebral ischemia in aneurysmal subarachnoid hemorrhage: a systematic review and meta-analysis. *Am J Neuroradiol*. doi:10.3174/ajnr.A3787
- Mills JN, Mehta V, Russin J et al (2013) Advanced imaging modalities in the detection of cerebral vasospasm. *Neurol Res Int* 2013, e415960. doi:10.1155/2013/415960
- Essig M, Shiroishi MS, Nguyen TB et al (2013) Perfusion MRI: the five most frequently asked technical questions. *AJR Am J Roentgenol* 200:24–34. doi:10.2214/AJR.12.9543
- Fieselmann A, Ganguly A, Deuerling-Zheng Y et al (2012) Interventional 4-D C-Arm CT perfusion imaging using interleaved scanning and partial reconstruction interpolation. *IEEE Trans Med Imaging* 31:892–906. doi:10.1109/TMI.2011.2181531
- Royalty K, Manhart M, Pulfer K et al (2013) C-Arm CT measurement of cerebral blood volume and cerebral blood flow using a novel high-speed acquisition and a single intravenous contrast injection. *Am J Neuroradiol* 34:2131–2138. doi:10.3174/ajnr.A3536